Available online at www.sciencedirect.com

jmr&t Journal of Materials Research and Technology

journal homepage: www.elsevier.com/locate/jmrt

Original Article

MgB_2-based biodegradable materials for orthopedic implants

P. Badica [a,*], N.D. Batalu [b,***], E. Balint [c,d], N. Tudor [c,**], F. Barbuceanu [c,e], A. Peteoaca [c], C. Micsa [c], A.D. Eremia [c], O.I. Trancau [f], M. Burdusel [a], M.A. Grigoroscuta [a], G.V. Aldica [a], D. Radu [a], I. Porosnicu [g], I. Tiseanu [g]

[a] National Institute of Materials Physics, Street Atomistilor 405A, 077125, Magurele, Romania
[b] University Politehnica of Bucharest, Splaiul Independentei 313, 060042, Bucharest, Romania
[c] University of Agronomic Sciences and Veterinary Medicine of Bucharest, 59 Marasti Boulevard, 011464, Bucharest, Romania
[d] "One Health – New Medical Concept" Association, 34-36 Nicolae Iorga Street, 010433, Bucharest, Romania
[e] Institute for Diagnosis and Animal Health, 63 Dr. Staicovici Street, 050557, Bucharest, Romania
[f] University of Medicine and Pharmacy "Carol Davila", Bd. Eroii Sanitari 8, Bucharest, Romania
[g] National Institute of Lasers, Plasma and Radiation Physics, Street Atomistilor 409, 077125, Magurele, Romania

ARTICLE INFO

Article history:
Received 11 May 2022
Accepted 27 July 2022
Available online 2 August 2022

Keywords:
MgB_2
Biodegradable
PLA
In vivo
Rat model
Bone interaction

ABSTRACT

Bulk high density MgB_2 and a composite material made of a PLA matrix and MgB_2 powder inclusions were *in vivo* tested as candidates for biodegradable materials for orthopedic implants. A rat model was used. Implants were introduced into femoral bone, in transversal and longitudinal directions. Assessment of the implant–tissue interaction was performed by X-ray imaging, X-ray computer tomography, electron microscopy, cytology, and histopathology on samples at 40 and 90 days after surgery. Both materials are biocompatible, bone and adjacent soft tissue showing good tolerance of implants. Biodegradation of MgB_2 is faster than for PLA-MgB_2 composite, but in both cases, it is accompanied by bone regeneration. Results suggest that use of MgB_2-containing composites can promote space and time control of degradation and promotes MgB_2 as a promising material for fracture repair.

1. Introduction

Implants can largely be classified as bioinert and biodegradable/bioactive types. Most common bioinert materials, often used for permanent or long period implants, are Ti and Ti-based alloys, stainless steels (316 L), Co–Cr alloys, ZrO_2 and Al_2O_3 ceramics. Materials used for biodegradable/bioactive implants are Mg/Fe/Zn-based alloys, and polymers, such as

* Corresponding author.
** Corresponding author.
*** Corresponding author.
E-mail addresses: petre.badica@infim.ro, badica2003@yahoo.com (P. Badica), dan.batalu@upb.ro (N.D. Batalu), nghtudor@yahoo.com (N. Tudor).

https://doi.org/10.1016/j.jmrt.2022.07.164

PLA/PLLA. New composite materials with hydroxyapatite are also emerging [1]. In orthopedics, most implants are made of bioinert materials.

Since 2019, a biodegradable material was approved by the EU and other countries [2]. Commercially known as MAGNEZIX, it is a Mg-based alloy with additions of Zr and rare earth elements [3]. This biodegradable material is used to fabricate simple orthopedic implants, such as screws, pins, and orthopedic clamps. These products successfully replace, in some cases, the bioinert materials. MAGNEZIX products are suitable for the bones of the elbow, hip, hand, shoulder, knee, ankle, and foot [2], usually as small parts that bear low loads. Other potential magnesium-based products recently tested *in vivo* are clips for laryngeal microsurgery [4], plates and nails [5], and wound-closing devices [6]. Mg-based alloys are currently studied as promising biodegradable implants and different review articles cover these materials, emphasizing their advantages and problems [7–10]. Criteria for a biodegradable material to be used for an implant are [11]: (*i*) biocompatibility, (*ii*) controlled biodegradability, (*iii*) suitable mechanical properties, and (*iv*) low cost. Another important aspect is *customization* and *adaptability* of the orthopedic implants depending on the patient condition, e.g., size, weight, gender, age, fracture specifics.

In this work, we present *in vivo* test results on a rat model for assessment of MgB_2-based materials as a new candidate for orthopedic biodegradable implants. Arguments in favor of considering this material for orthopedic applications are addressed in the following paragraphs.

Regarding the biocompatibility, the first criterion, Mg and some Mg-alloys have shown excellent biocompatibility without signs of allergic or toxic reactions, being characterized by a safe degradation [12–18]. Magnesium also provides infection inhibiting effects [19]. Furthermore, MgB_2 nanosheets have also proved to have a good osteogenic potential for bone disease-related therapeutics, since they are able to enhance the osteoblast differentiation of mouse mesenchymal stem cells when embedded in polymeric scaffolds [20]. The alkaline pH of Mg in water is reaching a value of ~11. Bulk MgB_2 with or without additions has a lower pH of ~8.5–10 [21,22] which is lower than that of pristine Mg, and closer to the blood pH ~7.4. The daily intake of Mg is 240–420 mg/day [11] and of B is 1–7 mg/day [23]. Mg is the fourth most abundant cation in the human body [24]. In healthy people boron levels are 15–80 μg/kg [25], being present in the body as boric acid, and it is completely absorbed from the gastrointestinal tract [26]. Magnesium [10] and boron [27–30] are involved in healthy bone growth and cell membrane care. The cytotoxicity of MgB_2 powders on different cellular lines was studied in [22,31,32]. While this is useful information, for biodegradable alloys, dynamic effects are important and only *in vivo* tests are relevant to observe if the body can accommodate the effects of the material implantation. MgB_2 has been shown to be an antimicrobial material [21,22,32]. This can be another useful feature to prevent soft tissue or bone infections [3]. From the biocompatibility and bioactivity viewpoints, MgB_2-based materials are expected to show similarities to Mg-based alloys, but synergetic effects induced by the presence of both B and Mg are not excluded.

Considering the second criterion concerns *biodegradation* aspects, many Mg-based alloys show a relatively high degradation rate in simulated body fluids at 37 °C, in many cases higher than the threshold of 0.5 mm/year proposed in ref. [33]. However, alloying and use of advanced technologies improve the corrosion resistance of biodegradable Mg alloys [9,34]. Previously performed studies indicate the MgB_2 corrosion rates in water of $4 \cdot 10^{-4}$ mm/year and of $4 \cdot 10^{-2}$–$3 \cdot 10^{-6}$ mm/year for MgB_2 added with Eu_2O_3 [21]. The presence of Cl^-, HPO_4^{2-}, and $H_2PO_4^-$ ions [35,36] in the phosphate-buffered saline solution accelerates Mg reaction and MgB_2 decomposition. The bulk density influences mechanical properties. The density of the bone is 0.92–2 g/cm^3 [37], the lower limit being for cancellous bone, and the upper one for the cortical bone, while the theoretical density of MgB_2 is 2.63 g/cm^3. Variation of the mechanical properties in correlation with the density of MgB_2 samples was studied by Murakami [38]. The Young modulus measured in the bending test was 311, 225 and 50 GPa when the packing ratio was 98, 92 and 63%, respectively (bending strength of 223–450 MPa). Therefore, during biodegradation, the mechanical properties of MgB_2 evolve towards those of the bone (Young modulus of 6–45 GPa, yield strength 120 MPa, compression/bending strength of ~250 MPa, ultimate tensile strength of 150 MPa, elongation strain 1.5–3% [11]). Another major concern is hydrogen gas release during degradation of Mg-based alloys for orthopedic applications. This can be potentially harmful [39] because the bone is poorly vascularized, and the natural removal of the hydrogen gas formed in the reaction between Mg and water and accumulated in the adjacent soft tissue as gas pockets, is slow. To suppress this effect, the Mg content can be decreased in the implant material. In this context, the MgB_2 with a high amount of B relative to Mg can be a promising solution vs. Mg-rich alloys. In summary, considering the as-presented biodegradation aspects, MgB_2-based materials may provide some advantages over Mg alloys.

The third criterion, *mechanical properties*, points out the necessity to match as much as possible the mechanical properties of the bone with those of the implant material. The biomechanical properties of MgB_2 are very similar to those of human bone [3]. Strength (tensile, compressive or yield) and elastic Young modulus are primary parameters. A large mismatch of elastic modulus can lead to the implant carrying a greater portion of the load and cause 'stress shielding' of the bone [40]. This incompatibility can generate early implant loosening, deterioration of the healing process, skeleton thickening, and chronic inflammation [41]. Some authors [33] consider that an elongation larger than 10% is also important, while strength should be above 200 MPa. Compressive strength of MgB_2 at failure point is 600–750 MPa [42] which is superior to Mg, Mg alloys, polymers, and bone and it is in the lower limit of Ti and Ti alloys [6,11]. The Young modulus of MgB_2 is 120–160 GPa [42], similar or slightly higher than the values for some high-strength Mg alloys and Ti alloys. Although a higher strength of MgB_2 when compared with Mg alloys and polymers is advantageous, MgB_2 is brittle, bearing similarities with ceramic rather than with metallic materials. The mechanical properties of MgB_2 can be considered intermediate among the biomaterials for orthopedic implants. At the same time, ceramic-like mechanical properties can be a

disadvantage since shaping of MgB_2 by conventional mechanical processing is not easy so that composites and certain fabrication technologies have to be considered, e.g. diffusion of Mg into a B powder compact [43,44].

The fourth criterion is *cost*. A biodegradable implant does not require a second surgery for implant removal, offering patients a faster healing, cost-effective and safer recovery (lower risk of infection). Quality of treatment increases, the duration of sickness decreases, and savings in the healthcare system increase (e.g. resources and time of the surgeons).

The state-of-the art and presented comparative analysis suggest MgB_2-based materials as possible candidates for fabrication of biodegradable orthopedic implants, worth to be investigated. In this study, implants were made of highly dense sintered MgB_2 bars and composite rods of PLA-matrix added with MgB_2 powder. *In vivo* tests have shown promising results recommending MgB_2 for biodegradable orthopedic applications.

2. Experimental

2.1. Materials and processing

Raw powder of MgB_2 was supplied by LTS Research Laboratories Inc (US). The powder was characterized in detail in ref. [22]. According to X-ray diffraction it consists of 97 wt. % MgB_2, the main phase, and of 1.8 wt. % MgO and 1.2 wt. % Mg, the secondary phases (Fig. 1).

Disks of 20 mm diameter and 3 mm thickness were prepared by Spark Plasma Sintering (SPS) at 1150 °C, for 3 min. Details of processing and characterization were reported in ref. [45]. According to X-ray diffraction, in sintered material, phase composition modified to 87.5 wt. % MgB_2, 8.6 wt. % MgO, and 3.9 wt. % MgB_4 (Fig. 1). One observes that the implant material is a composite, and each component is expected to influence implant behavior in the biological environment.

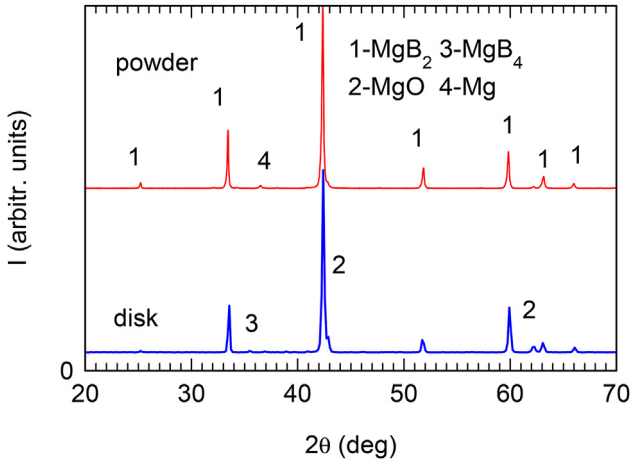

Fig. 1 – XRD patterns normalized to the most intense peak of MgB_2 (2θ ~ 42.41°) of the raw MgB_2 powder and of the sintered MgB_2 bulk. Phases are: 1 - MgB_2 (ICDD 72–7019), 2 - MgO (ICDD 45–0946), 3 - MgB_4 (ICDD 73–1014), and 4 - Mg (ICDD 35–0821).

Though important, this aspect is beyond the purpose of the current work. Relative bulk density of the sintered MgB_2 measured by Archimedes method in toluene is high, about 99%. Disks were cut with a diamond saw into bars of 4 and 9 mm length, with a square cross-section of 1 mm edge (Fig. 2 a). After polishing all faces down to 1 μm of the diamond abrasive paste, the shorter bars were used for transversal implantation into the femoral bone, and the longer ones were placed in the longitudinal direction.

Composite filaments (1.5 mm in diameter and 15 mm long) of polylactic acid (PLA) containing MgB_2 powder were manufactured. The filament was made by dissolving PLA in dichloromethane and mixing the obtained solution with MgB_2 powder (20 wt. %). After pouring the solution on a flat metallic surface, the solvent was evaporated. The result was a 2–3 mm thick layer, which was cut into small fragments. The fragments were used to fabricate a filament with ~1.5 mm in diameter by hot extrusion at 180 °C on a Noztek extruder. Filaments were cut into small rod pieces with length of 4 and 9 mm (Fig. 2 b) and they were used as implants, similar to MgB_2 sintered bars addressed in the previous paragraph.

2.2. In vivo tests and methodology

The *in vivo* tests were performed in accordance with national and European legislation for animal protection, being approved by the Bioethics Commission of the University of Agronomic Sciences and Veterinary Medicine of Bucharest (19/09.11.2020) and authorized by Sanitary Veterinary and Food Safety Directorate of Bucharest (599/15.02.2021).

Sixteen healthy, 4 months old Wistar male rats, weighing 200–250 g were divided into 4 groups, each group consisting of 4 rats. The assessment of the bone reaction to the action of the implant (biocompatibility, biodegradation, bone regeneration) was performed at 40 and 90 days post-surgery. Two groups were used for the introduction of MgB_2 rods and two for PLA-MgB_2 rods. Groups and examples of implantation during surgery are presented in Table 1 and Fig. 3. The animals' food and water intake as well as social behavior were monitored for 14 days before the surgery.

The surgery was performed according to the previously established procedures [46–48]. Following preoperative clinical check-up, subcutaneous injection of 0.05 mg/kg atropine sulphate was administered 10 min before anesthesia.

All animals were anaesthetized for surgery with intramuscular injections of ketamine hydrochloride (20 mg/kg Vetaketam) and xylazine (2 mg/kg Xylazine 2%). While preparing each patient for surgery all the asepsis and antisepsis procedures were followed. Before implantation, all implant materials were UV sterilized. The sample rods were implanted intramedullary in the rats' femurs after predrilling with a 3 mm ball-shaped diamond bur fitted to a dental drill (part of a veterinary dental unit produced by Lingchen, China). In the first two groups, the femur was isolated, and the middle third was drilled with a diamond bur, simulating a longitudinal fracture in the compact femoral shaft. Through the obtained window, the implants (MgB_2 and PLA-MgB_2), with a length of 9 mm, were introduced. In the other two groups, the femur was transverse drilled. The introduction of the MgB_2 or PLA-MgB_2 (4 mm in length) biodegradable implants through the

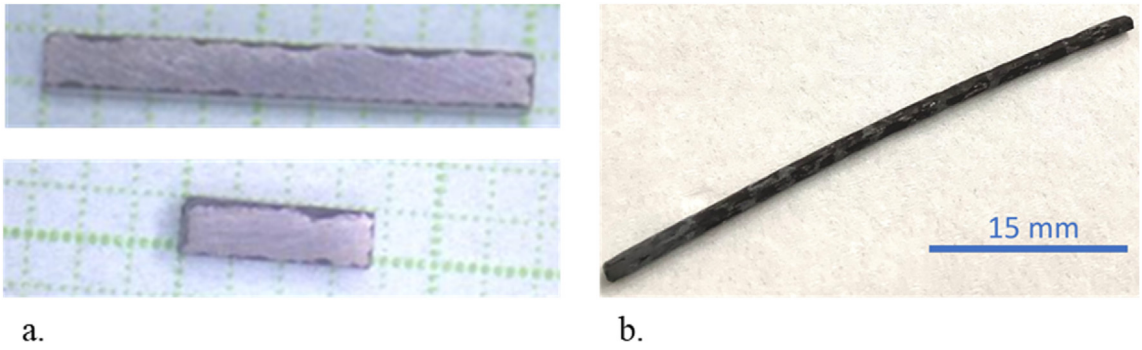

Fig. 2 – Images of MgB_2 sintered bars (a) and of PLA-MgB_2 filament (b) cut in small rods and used as implants into femoral bone of the rat model (see section 2.2).

compact bone, through the medulla was performed to monitor its interaction with both bone tissue and adjacent soft tissues.

After the surgery, the body temperature was monitored and adjusted by using a heating pad at 37 °C until the end of anesthesia. All rats received a subcutaneous injection of Enrofloxacin (10 mg/kg Enrofloxacina 2.5%) as antibiotic prophylaxis and a subcutaneous injection of glucose solution for rehydration (2.0 ml Glucose 5%).

To observe the biocompatibility, biodegradation, and bone regeneration processes of the implanted materials, the animals were evaluated postoperatively at 40 and 90 days by imaging examination, cytology, and histopathology. Available residuals of implants were extracted and studied.

Radiological X-ray imaging was made with DuraDiagnost F30 machine (Philips, China) on sedated rats. Two radiological views of the implant limbs (medio-lateral and cranio-caudal) were performed on the rats in lateral and dorsal recumbency. The source-receptor distance was 100 cm, and no grid was applied. All obtained images were analyzed using the DICOM-viewer software (Pixeldata, Romania). It is noteworthy that the implant material contains elements with small atomic numbers (Mg^{12} and B^5) so that the implant is relatively radiotransparent (especially for PLA-MgB_2 composite rods) and, thus, it is difficult to observe details. The observations were supplemented with images obtained by X-ray computer tomography (XCT).

Table 1 – Rats groups undergoing femoral implantation surgery.

Group	Implantation of pristine MgB_2 bars and PLA-MgB_2 composite rods
1	MgB_2 sintered bar implanted longitudinally intramedullary in the femur
2	PLA-MgB_2 rod implanted longitudinally intramedullary in the femur
3	MgB_2 sintered bar implanted transversely through compact bone and muscle tissue
4	PLA-MgB_2 rod implanted transversely through compact bone and muscle tissue

For the cytological examination, the sampling was performed using the medullary puncture technique on all subjects. The fine needle aspiration was made at the level of the proximal femoral epiphysis. The aspirated material was smeared on multiple glass microscope slides (medullograms) and then stained using the panoptic staining technique (May Grunwald-Giemsa/Romanovsky/Pappenheim, MGG) [49–53].

To describe post-implant histopathological changes, the bone tissue samples were immediately fixed in Baker solution and subsequently in the decalcification solution. After decalcification, bone tissue samples were incorporated into Paraplast Plus (Sigma) embedding medium by using the HISTOS 5 semi-automatic dehydration and paraffin embedding device. Paraffin sections (5 μm) were deparaffinized, usually stained with the Hematoxylin-Eosin (HE) method [54]. The examination of both cytological smears and permanent stained histological preparations was performed with Olympus BX 51 DP-soft and Camedia-soft Microscope, at magnifications of 40×, 100x, 200x, 400x, and 1000x.

2.3. *Characterization techniques*

Materials before and after implantation were investigated by different techniques.

A Bruker-AXS D8 ADVANCE powder diffractometer ($Cu_{K\alpha 1}$ radiation, $\lambda = 1.5406$ Å) was used for X-ray diffraction (XRD) patterns.

Images of microstructure and the local maps of elements were taken by scanning electron microscopy (SEM/EDX, Tescan Lyra 3).

X-ray computer microtomography (XCT) analysis was performed with an in-lab built micro-tomograph [55,56]. Briefly, the computer tomography (CT) configuration includes an X-ray tube (YXLON) that can operate at a voltage up to 225 kV and a maximum target power of 15 W. The images were acquired with a PerkinElmer flat panel X ray detector (2000 × 2000 px, pixel size = 200 μm, 16 bit) working in the binning 1 × 1 regime. The integration time for each radiographic images was set to 1 s and two images were averaged before data storage. Samples were scanned in identical condition at a voltage of 90 kV and a current of 160 μA, using 1.5 mm Al filtration. The incremental step between radiographies was 0.2° and a total of 1800 projections were acquired. The 3D model was reconstructed in cone-beam CT

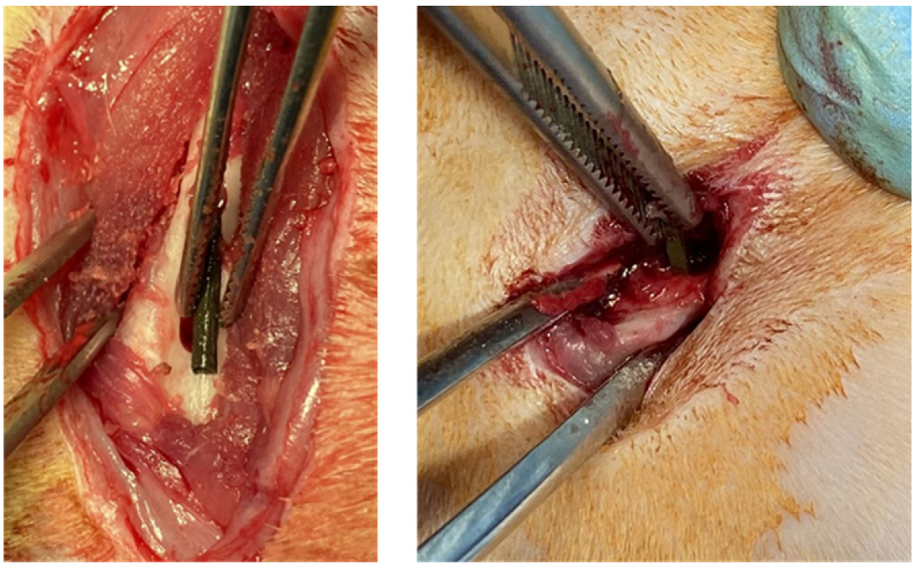

Fig. 3 – Images taken during implantation surgery: (a) Groups 1–2: intramedullary introduction of the longitudinal MgB_2/PLA-MgB_2 implant; (b) Groups 3–4: transversely implantation of MgB_2/PLA-MgB_2 to the bone, through the compact bone and muscle tissue.

configuration using filtered back-projection algorithm provided by the Volume Graphics Software (VGStudio Max 3.5.0) obtaining a nominal voxel of 20 μm.

3. Results and discussion

3.1. *Materials aspects after extraction*

After 40 days of implantation, the MgB_2 implant consists of several large pieces indicating that biodegradation occurred. The main part, although porous, showed some shape and mechanical integrity (Fig. 4a). However, there are strongly affected cross sections in which the compact core has a diameter of less than 200 μm (Fig. 4b), although the total apparent diameter is 0.5–0.8 mm. Other details of much interest can be observed. An image in the cross section of the implant bar indicates that in different areas 40–50% of the initial diameter has been resorbed (Fig. 4c). The bioresorption process is not uniform. It is remarkable that in the images of Fig. 4c and d the bone can be seen on the surface of the implant. In some areas, the implant and the bone form a common unitary body, difficult to separate. This result indicates an osseointegration process. Elemental EDS maps (Fig. 5) support these results by the fact that elements composing the respective bone (Ca, Na, K, P and Cl) were detected in the extracted implant. Similar results were obtained for the MgB_2 transversal implant (Group 3, Table 1) at 40 days.

At 90 days after implantation (Groups 1 and 3, Table 1), degradation of MgB_2 was in a more advanced stage and only some powder-like fragments were observed (see Section 3.2).

A much slower corrosion (Fig. 6) was encountered in the *in vivo* experiments where the implant was the composite PLA-MgB_2 rod (Groups 2 and 4, Table 1). At 40 days after implantation, the surface of the implant is just starting to degrade and there is no bone adhered on its surface. There are some regions of preferential degradation developing on the surface of the composite.

When observing the cross section of the PLA-MgB_2 rod after 90 days, the PLA matrix has more pores than in the initial, as-prepared material before implantation surgery (compare SEM images a and b, d and h in Fig. 7). This result indicates that corrosive biodegradation of the PLA-MgB_2 implanted in the rat's femoral bone for 90 days took place in the rod's volume. Moreover, biodegradation of PLA-MgB_2 is apparently more uniform than in the case of the bulk MgB_2 implants (after 40 days) addressed in the previous paragraph, but a conclusion cannot be presented considering very different degradation rates of PLA (or PLA-MgB_2) and MgB_2, and more research is needed. Elemental EDX maps of Mg (Fig. 7 b and f) show the presence of this element in the initial PLA-MgB_2 rod and in the implanted material for 90 days. The red-green-blue (RGB) elemental maps (Fig. 7 c and g) obtained by overlapping the elemental maps for Mg, B, C, and O suggest that Mg is not free, and it forms compounds. Since EDX cannot detect hydrogen (expected to be present in compounds such as $Mg(OH)_2$, H_3BO_3 that may occur in the biodegradation process) and quantitative EDX analysis does not provide reliable data for light elements such as B, C, and O, it was not possible to ascribe a compound to a given region/grain in the PLA-MgB_2 composite samples. Biodegradation of MgB_2 from the PLA-MgB_2 is also supported by the color change of the rod. Initially the appearance of the rod was black, due to MgB_2 black powder embedded in the white PLA. After implantation for 90 days, the color became light gray, due to the mixing of possible reaction products, e.g. MgO (white), $Mg(OH)_2$ (white), B_2O_3 (white), H_3BO_3 (white), and B (black), and unreacted MgB_2 (black).

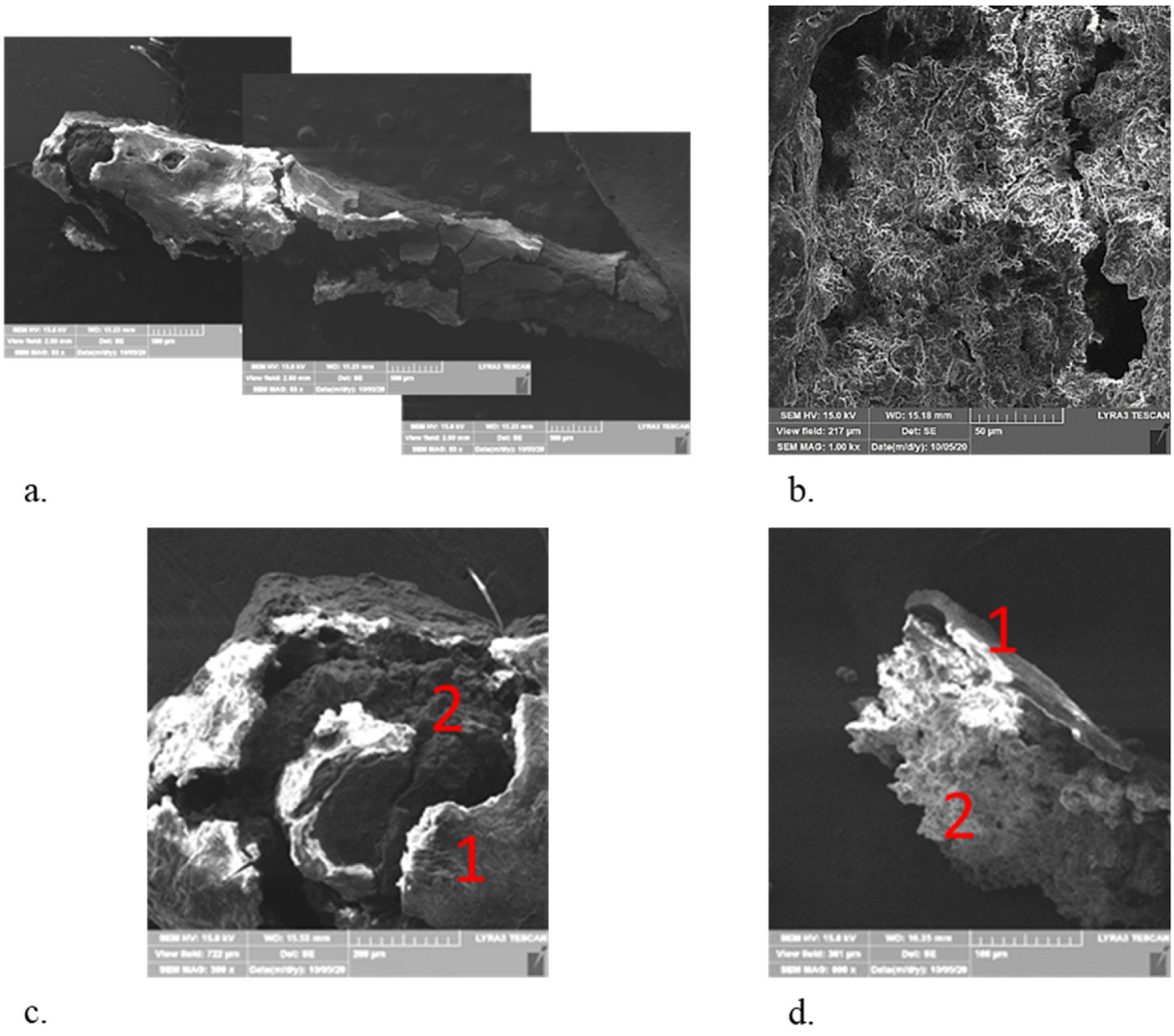

Fig. 4 – SEM images of the MgB_2 bar implant extracted from the femur of the rat model after 40 days of implantation: (a) general image; (b) core (cross section) of the extracted implant; (c) and (d) details of the implant showing bioresorption of the implant and attachment of the bone on it. Notations are: 1- bone attached to the implant, 2 - MgB_2 implant (Group 1, Table 1).

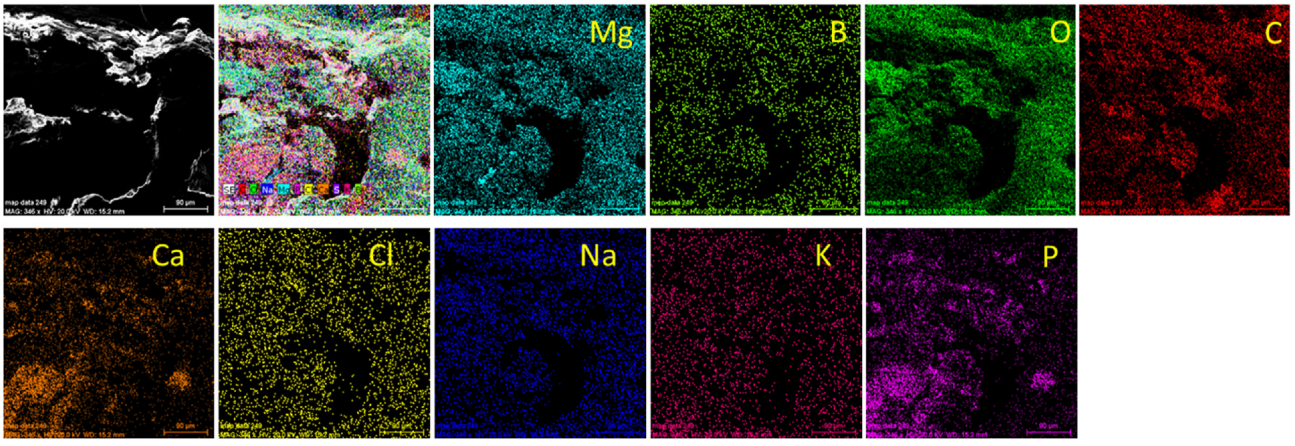

Fig. 5 – EDX maps of elements measured on cross section of MgB_2 extracted bar from the femur of the rat, after 40 days of implantation (Group 1, Table 1).

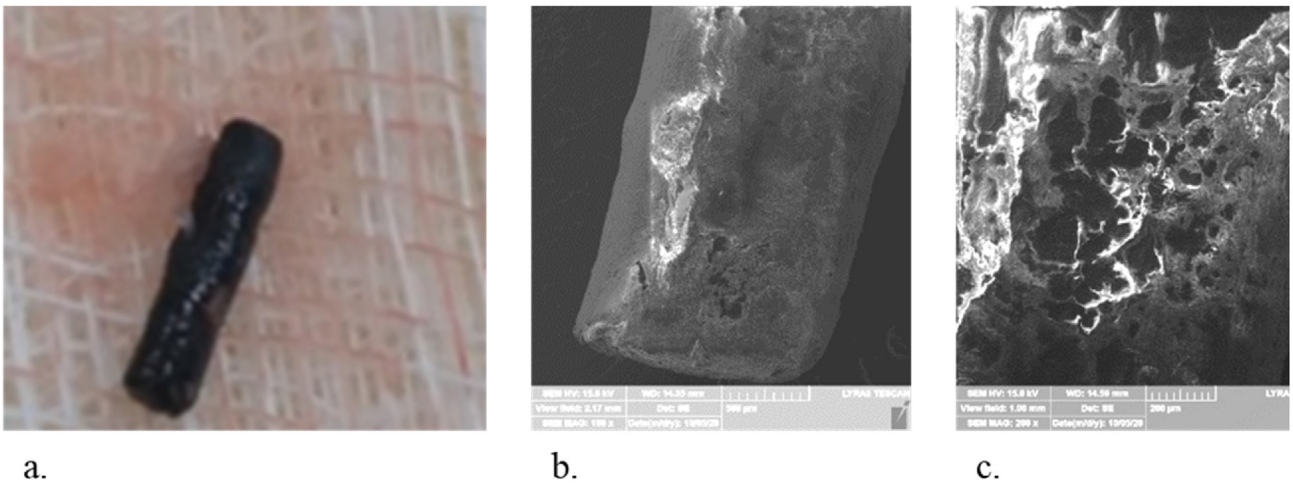

Fig. 6 – PLA-MgB_2 rod implants extracted from the rat's femur after 40 days of implantation: (a) transversely implanted (Group 4, Table 1); (b) and (c) SEM images of the longitudinally implanted rod taken at low and high magnification, respectively.

In summary, this section indicates the high potential of MgB_2 used for biodegradable bone implants. More details supporting these findings are presented in Section 3.2.

3.2. *Implant-bone interaction aspects by X-ray radiological and XCT observations*

A radiolucent area was observed at the MgB_2 implant site (after 15 and 40 days of implantation), representing the accumulation of hydrogen gas (Fig. 8 a, arrow sign). The result is consistent with other *in vivo* studies on Mg-based materials implanted into bone [57]. However, Witte et al. [57] observed that gas accumulation disappeared after 2–3 weeks from intervention, whereas in our work, gas pockets were still present at 40 days, but reduced in quantity (when compared to 15 days, not shown). The amount of gas was higher for MgB_2 implants (40 days) inserted longitudinally than for those inserted transversely (Fig. 8 a, b) and this can be explained by

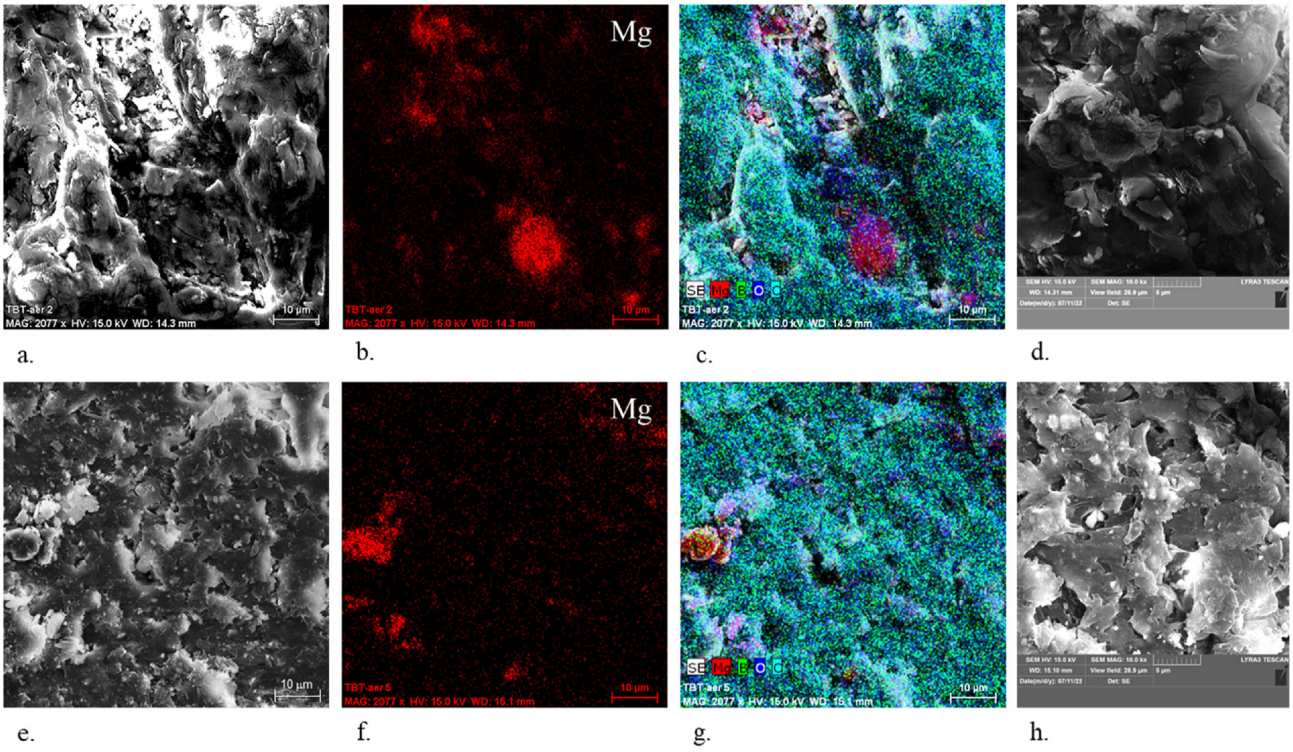

Fig. 7 – SEM/EDX images taken on PLA-MgB_2 rods before (a–d) and after longitudinal implantation (Group 2, Table 1) for 90 days (e–h).

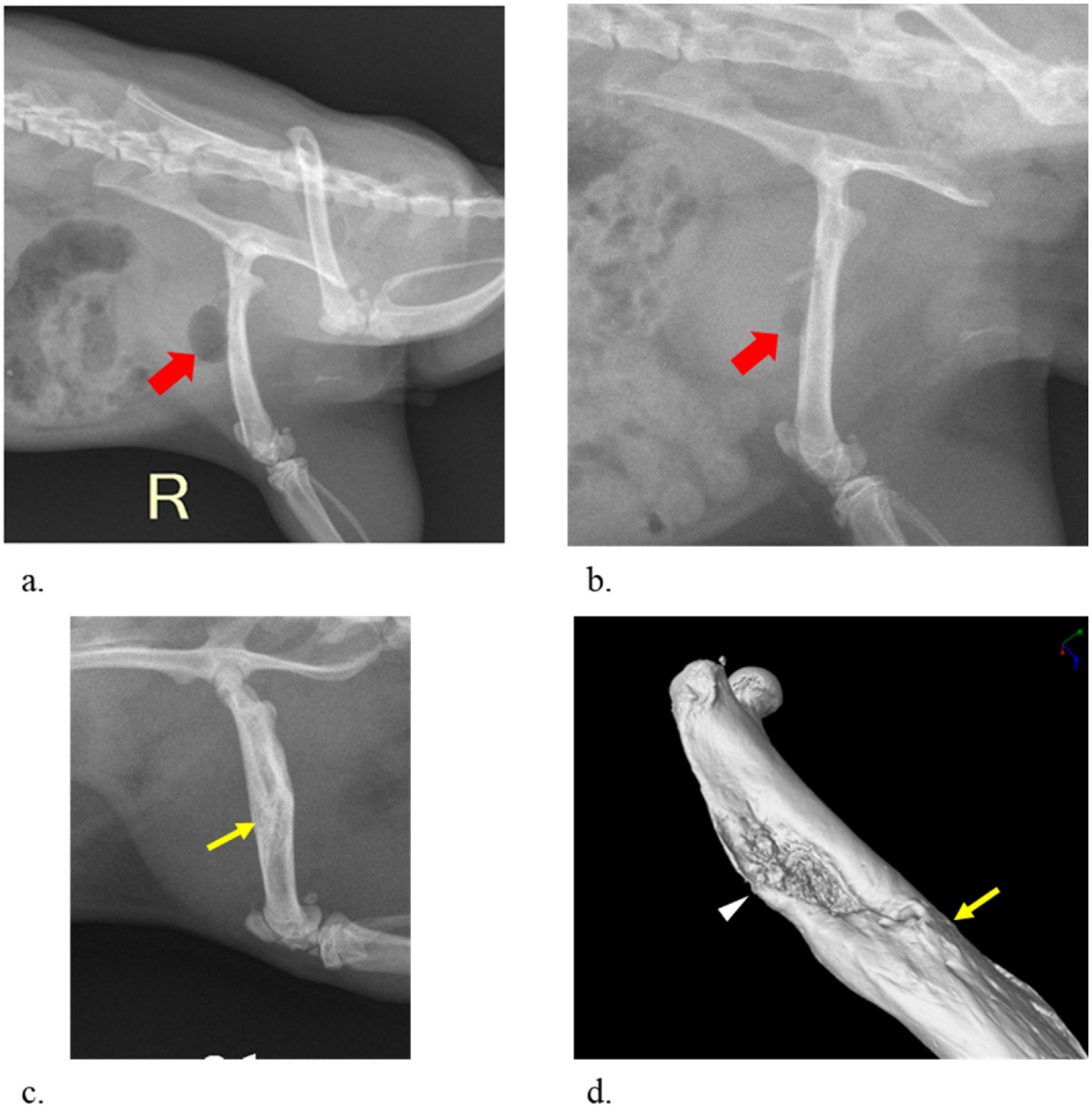

Fig. 8 – Radiological X-ray images taken on the rat models with: (a) MgB_2 longitudinal implant at 40 days; (b) MgB_2 transversal implant at 40 days; (c) MgB_2 longitudinal implant at 90 days; (d) XCT 3D reconstruction image on proximal extremity of the femur with MgB_2 implant at 90 days. Note: in (a) and (b) the presence of H_2-gas pockets (indicated with thick red arrows) and lack of the gas accumulation in (c). Also observe in (c) the partial repair of the fracture site (thin yellow arrow); XCT 3D reconstruction image in (d) shows the presence of callus (white arrowhead) and bone remodelling (thin yellow arrow) at the site of implantation.

the higher amount of the implant material in the longitudinal case than in the transversal one. At 90 days after implantation gas pockets were not observed (Fig. 8 c) meaning that gas was fully resorbed.

Before going into other bone-implant interaction details, it is worthy to note that in some situations there was a total fracture of the femoral shaft, due to the bone physiological thinness, and the species behavior. The total fracture allowed the bone heads to move, but in most cases still there was a fibrous callus that later mineralized, succeeding in repairing the fracture site. At 40 days after surgery, the presence of a slight periosteal reaction was found. At 90 days, no significant bone changes were observed at the site of implant, and no bulk implant material was revealed suggesting that MgB_2 was decomposed and resorbed. Even in the case of total fractures, both X-ray examination and XRT show evidence of healing at the fracture site (Fig. 8 c, d), although no measures of immobilization of the resulting bone fragments were applied.

For the PLA-MgB_2 composite implant we could not observe any gas accumulation after 40 and 90 days (Fig. 9 a, b), due to the lower rate of degradation of the composite material (see Section 3.1) and lower amount of the MgB_2 component (20 wt. %). According to radiographic examination performed, after 40 days of implantation no remarkable changes were observed,

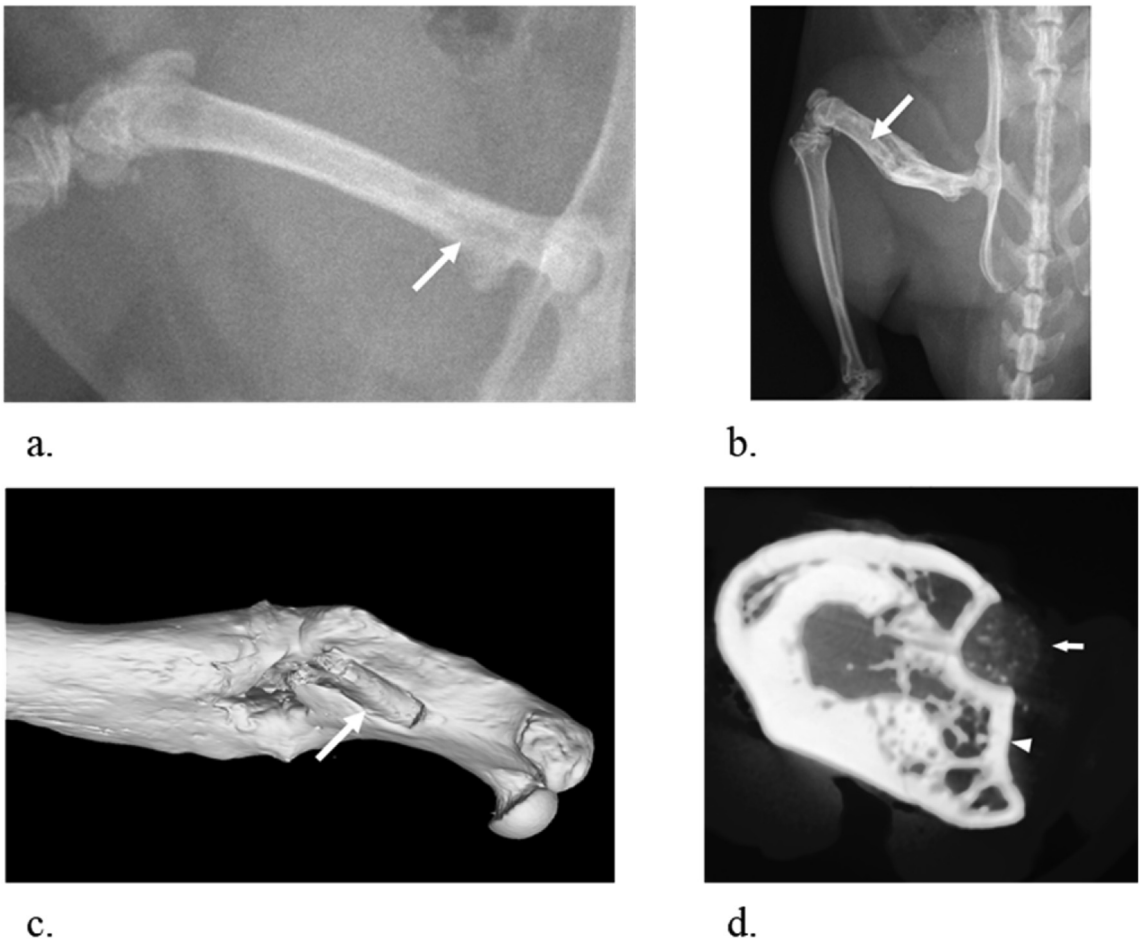

Fig. 9 – Radiological X-ray images taken on the rat models with: (a) PLA-MgB_2 transversal implant at 40 days; (b) PLA-MgB_2 longitudinal implant at 90 days; (c) XCT images on femur with PLA-MgB_2 longitudinal implant at 90 days from (b); (d) cross sectional CT view showing callus formed (arrowhead) with embedded implant (white arrows) outside the medullary channel.

only a slight periosteal reaction in some cases, demonstrating a good tolerance of the bone towards the implanted material (Fig. 9 a). Also, at 90 days by radiographic and XCT examinations no other visible special changes were noticed (Fig. 9 b, c, d): callus forms and the integrity of the PLA-MgB_2 implant is preserved. These observations confirm slow biodegradation of PLA-MgB_2. However, the XCT images from Fig. 9 c, d indicate for the selected specimen that calcification of the fracture site is defective and, thus, produces angulation due to lack of bone-fragments immobilization. Angulation of the bone is easily observed in the radiography from Fig. 9 b. One also notes that the implant is embedded in the callus and migrated outside the medullary canal (Fig. 9 c, d).

As noted in ref. [3] the MAGNEZIX implants generate a low interference of the signals, hence, the artefacts due to implant are minimum and this improves the diagnosis and the ability of surgeons and radiologists to assess the images [3]. Implants that contain MgB_2 show similar useful features [3].

3.3. *Histopathological and cytopathological examination*

For Groups 1 and 3, the histopathological examination at 40 days shows necrosis processes of the micro bone fragments produced while drilling, due to the traumatic process of penetration of the rods into the medullary channel (Fig. 10 a, b), and uneven micro-thickening of the periosteum (Fig. 10 c). This fact caused the hematopoietic marrow to react by producing micro-hemorrhages and to cause a cell proliferation on various cell lines (lymphohistiocytic, myelocytic, mast cell; Fig. 10 d, e). This proliferation phenomenon can be well visualized and confirmed by cytological examination (Fig. 10 f, g). Histopathological examination brings also clear evidence of MgB_2 implant degradation: powder particles were detected in the muscle tissue and periosteum (Fig. 10 d, e).

At 90 days after implantation, bone compact microfragments, micro-hemorrhages and lymphomacrophagous cell infiltrates have occurred in the impact areas of the sintered MgB_2 implant (Fig. 11 a). The implanted sintered MgB_2 bars were fully decomposed, and a strong resorption process occurred. The evidence of implant degradation is the presence of powder particles in the bone compact and in the bone marrow (Fig. 11 c). An important histopathological change observed at 90 days after implantation is the appearance of a tissue reactivity reflected by fibrosis and collagen formation (conjunctive–fibrous reaction, Fig. 11 b). Another relevant change is observed in the bone marrow by the presence of

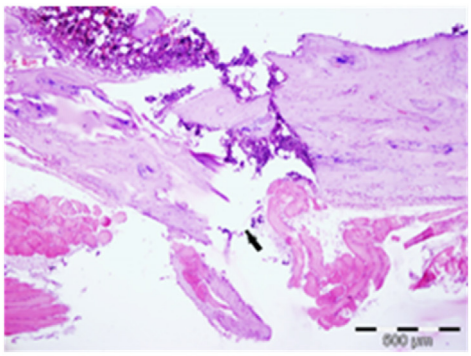

a.

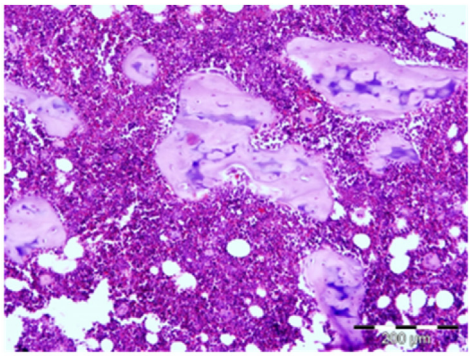

b.

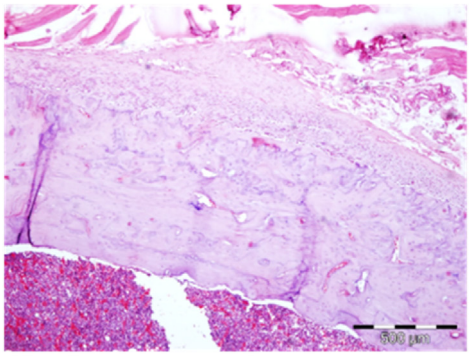

c.

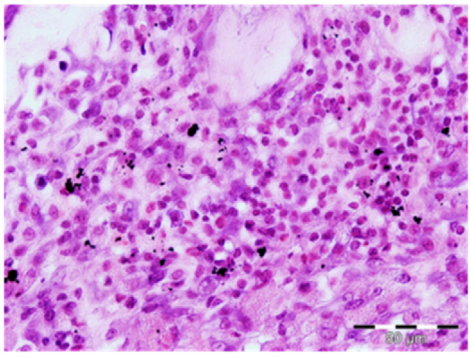

d.

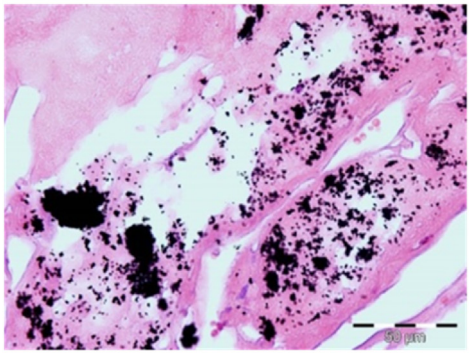

e.

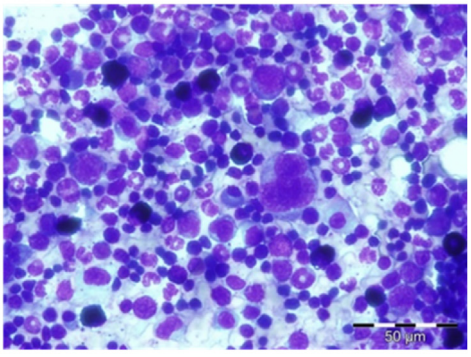

f.

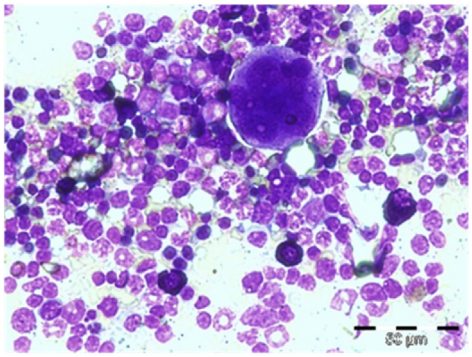

g.

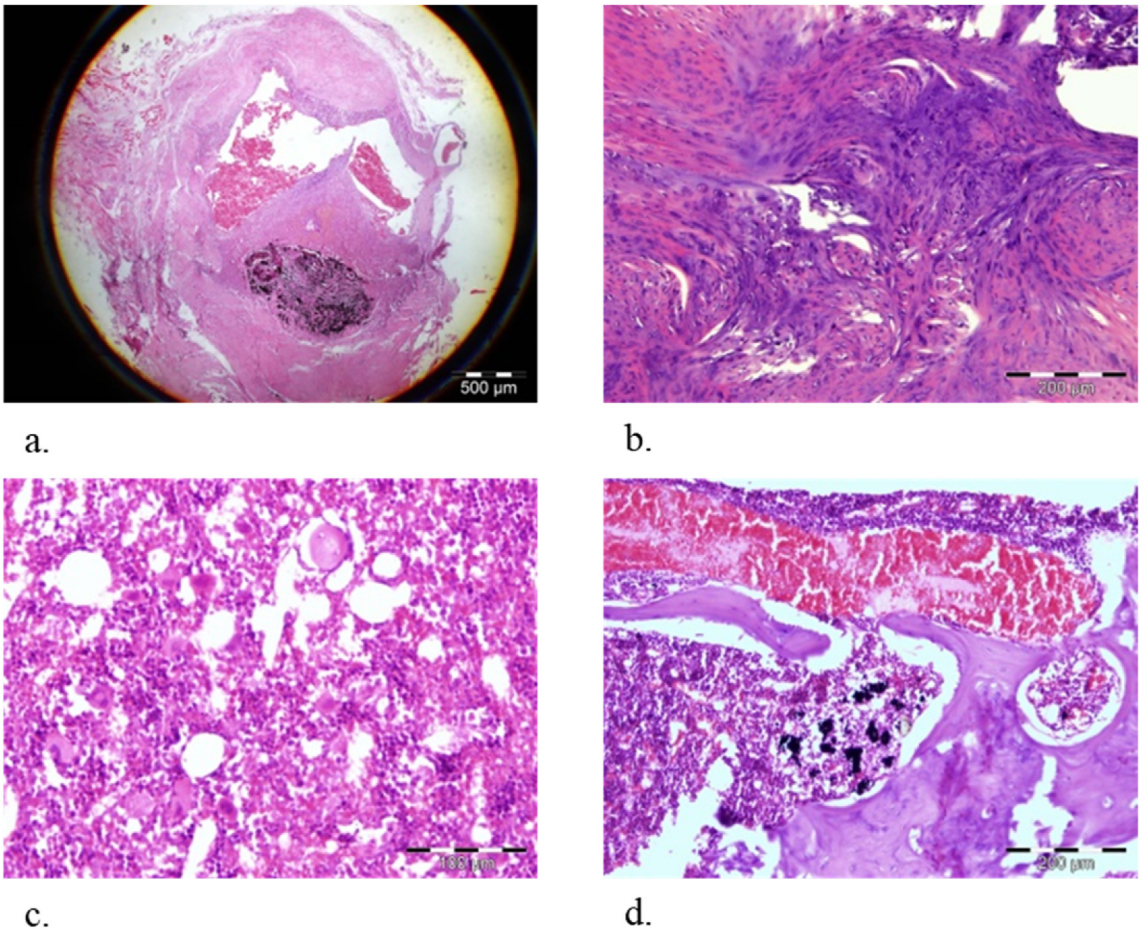

Fig. 11 – Histopathological and cytopathological observations on samples for the MgB_2 implant after 90 day of surgery: (a) overview showing increased tissue reactivity, fibrosis and cellular reaction around the implant (HE staining, 12.5x); (b) fibrosis and collagenization area (HE staining, 200x); (c) hematogenous bone marrow with the presence of osteoblasts and osteoclasts (HE staining, 200x); (d) trabecular-shaped bone compact with inorganic particles and bone marrow micro-hemorrhages (HE staining, 100x).

osteoblast and osteoclast cells that prove the process of bone regeneration (Fig. 11 d).

At 40 days, PLA-MgB_2 composite implants preserved their integrity being easily recovered. However, histopathological examination indicates the implant degradation. Degradation is related to MgB_2 particles dispersed in the PLA-MgB_2 composite, remnants of powder particles being found in the adjacent soft tissue to the implanted bone (Fig. 12 a), but the PLA rod was still in the bone. Degradation of the PLA-MgB_2 composite occurs and it is slower compared to pristine MgB_2 implant. This suggests that different amounts of MgB_2 in the polymer can provide a controlled biodegradation rate of the PLA-MgB_2 implant, but further research is required to demonstrate this idea. The lesions at the contact site with the PLA-MgB_2 implant were the same as with the MgB_2 ones (bone micro scales, bone compact deformation, micro hemorrhages, Fig. 12 b). Histopathological examination of the bone marrow showed increased cellular reactivity with the presence of osteoblasts and osteoclasts (Fig. 12 c). Cytopathological examination at the medullary level confirmed, through the presence of young cells of all cell lines (Fig. 12 d, e, f) that, together, these cells participate in bone regeneration.

Fig. 10 – Histopathological and cytopathological observations on samples for the MgB_2 implant after 40 days of surgery: (a) implantation area showing micro-fragments of the compact bone and micro-scales formation and marrow cell reaction (HE staining, 40x); (b) reactive hematogenous marrow showing increased cellularity and numerous necrotic bone microscales (HE staining, 100x); (c) uneven thickening with multi-lamellar appearance of the periosteum (HE staining, 40x); (d) MgB_2 microparticles present in the structure of the periosteum and lymphohistiocytic cell proliferation (HE staining, 400x); (e) inorganic particles with different shapes and sizes, randomly arranged, isolated or forming aggregates in the muscle fibers; (f) spinal cord hyperplasia - all cell lines normally represented, except mast cell hyperplasia (MGG staining, 40x); (g) osteoclasts surrounded by elements of the lymphoreticular system and mast cells (MGG staining, 40x).

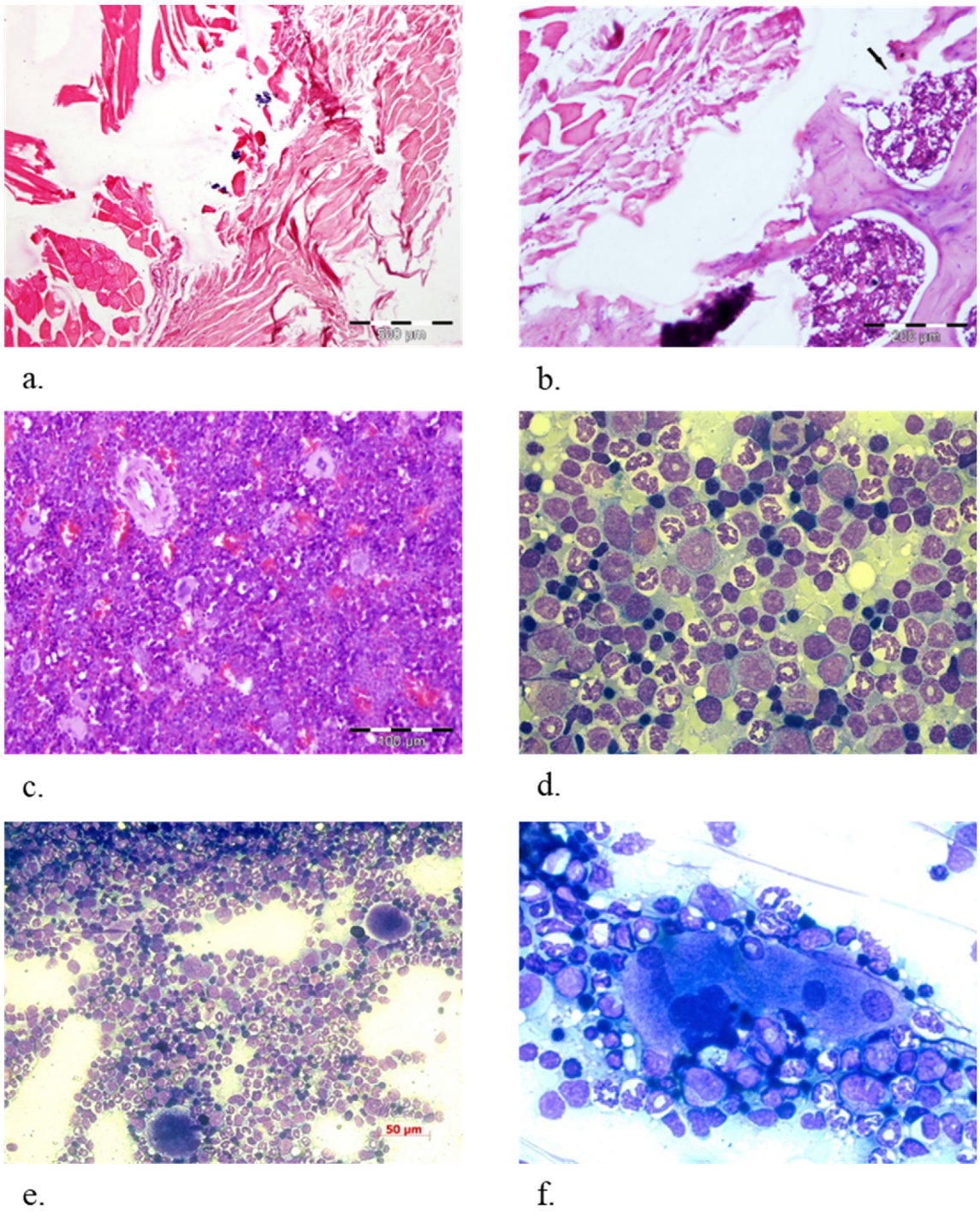

Fig. 12 – Histopathological and cytopathological observations on samples of composite PLA-MgB_2 implant after 40 days of surgery: (a) striated muscle fibers, adjacent to the bone radius, torn with the presence of particles/agglomerates (HE staining, 40x); (b) implant area showing compact tunnelling with the formation of microscales and disorganization of the Havers channels indicated with the arrow (HE staining, 100x); (c) reactive hematogenous marrow with pleomorphic cellularity, numerous osteoclasts and osteoblasts (HE staining, 200x); (d) medullogram showing young elements of the erythrocyte series (erythroblasts) of the myelocyte series (promyelocytes, myelocytes) and lymphocytes highlighting the regenerative process at the medullary level (MGG staining, 100x); (e) medullogram showing megakaryocyte (top) and osteoclast (bottom) surrounded by young elements of the erythrocyte and monocyte series (MGG staining, 100x); (f) detail presenting a multinucleated bone cell (osteoclast), surrounded by mononuclear and polymorphonuclear cells (MGG staining, 100x).

90 days after implantation of PLA-MgB_2 in rats, no histopathological changes were found other than those revealed at 40 days after implantation.

Bio assessment of PLA-MgB_2 composite from this work comply with other excellent results obtained for PLA-based biodegradable/bioresorbable composites tested *in vitro* or *in vivo* for orthopedic applications [58–62]. These materials show a multifunctional useful biomechanical behavior with possibilities of properties control depending on patient's needs. Furthermore, many of the PLA-based composites overcome the drawback of relatively weak mechanical properties of PLA and are easy to processes, e.g. by 3D printing into complex, innovative, and customizable bone implants/scaffolds/joints/regeneration membranes. A direct comparative analysis between different PLA-based composites is not straightforward due to complexity, different aims, and evaluation conditions. Further research is required to provide optimum solutions for bone engineering.

4. Conclusion

Two types of biodegradable materials for orthopedic implants, MgB_2 and PLA-MgB_2, were assessed by *in vivo* tests of implantation into the femoral bone of the rat model. Implants were introduced longitudinally and transversally. Examination was performed by different techniques at 40 and 90 days after surgery. By imaging assessment of the MgB_2-implant groups, low gas accumulation that decreased over time was observed at the implant site. Also, a periosteal reaction was revealed. In the case of PLA-MgB_2 composite, the implant is more stable than MgB_2, showing slow degradation. Inorganic particles that resulted from disintegration of MgB_2 were found in the bone and muscle tissue for both types of implant materials. This indicates that corrosion in the PLA-MgB_2 composite takes place preferentially and faster at the MgB_2 sites. After 90 days from implantation, PLA-MgB_2 implants preserved their mechanical integrity and were easily extracted from the medullary channel of the bone. Presented results suggest the possibility to control the implant degradation in time and space by using composites with different amounts or gradients of PLA and MgB_2 components. Both materials demonstrated a good tolerance of the bone to the implanted material. At 40 and 90 days post-surgery, it was found that the implants used did not cause cellular dysplastic changes that over time could have generated neoplastic processes.

In conclusion, *in vivo* tests of the proposed materials show excellent biocompatibility, optimal biodegradation, and good tissue regeneration. Therefore, orthopedic implants based on MgB_2 for fractures repair can be envisioned in veterinary and human medicine.

CRediT author statement

PB – conceptualization, data curation, formal analysis, funding acquisition, investigation, methodology, project administration, resources, supervision, validation, visualization, writing - original draft, writing-review & editing; NDB – conceptualization, formal analysis, investigation, methodology, resources, validation, visualisation, writing-review&editing; EB – conceptualization, data curation, formal analysis, investigation, methodology, resources, supervision, validation, writing - original draft, writing - review&editing; NT– conceptualization, data curation, formal analysis, investigation, methodology, resources, supervision, validation, writing - original draft, writing-review&editing; FB – formal analysis, resources; AP – investigation, visualization; CM – investigation; ADE – investigation; IOT – writing-review & editing; MB – investigation; MAG – investigation, visualization; GVA – formal analysis, investigation, validation, writing-review & editing; DR – investigation; IP – formal analysis, investigation, visualization; IT – formal analysis, methodology, validation, resources.

Authors thank Prof. A. Tanase for his contribution in performing the surgical interventions and Dr. A. Popovici for his help in the preparation of histopathological samples.

In memoriam of Prof. N. Manolescu, a strong supporter of this work.

Declaration of Competing Interest

The authors declare that they have no known competing financial interests or personal relationships that could have appeared to influence the work reported in this paper.

Acknowledgments

P.B, N.D.B, M.B, M.A.G, G.V.A acknowledge Romanian National Authority for Scientific Research and Innovation (UEFISCDI), and EU for financial support, project 74-COFUND M– ERA.-NET" title="http://ERA.NET">ERA.NET II—BIOMB and 5PTE BIOTEHKER. The fee for open access publication was supported from the project 35PFE/2021, funded by the Romanian Ministry of Research, Innovation and Digitalization.

REFERENCES

[1] Pathak DK, Pandey PM. Evaluation of in vitro corrosion behavior of zinc–hydroxyapatite and zinc–hydroxya patite–iron as biodegradable composites. J Biomed Mater Res B 2021;109:436–50.
[2] https://www.engineeringnews.co.za/article/magnesium-bone-implants-gradually-replacing-titanium-implants-globally-2019-09-10/rep_id:4136 (accesed on 17.01; 2022.
[3] https://www.syntellix.de/en/products/technology.html (accesed on 17.01; 2022.
[4] Chang CB, Lau DP, Choo JQ, Chui CK. A bioabsorbable microclip for laryngeal microsurgery: design and evaluation. Acta Biomater 2012;8:2835–44.
[5] Waizy H, Seitz J-M, Reifenrath J, Weizbauer A, Bach F-W, Meyer-Lindenberg A, et al. Biodegradable magnesium implants for orthopedic applications. J Mater Sci 2013;48:39–50.
[6] Hänzi AC, Metlar A, Schinhammer M, Aguib H, Lüth TC, Löffler JF, et al. Biodegradable wound-closing devices for

gastrointestinal interventions: degradation performance of the magnesium tip. Mater Sci Eng C 2011;31:1098–100.
[7] Deshmukh RM, Kulkarni SS. A review on biomaterials in orthopedic bone plate application. Int J Eng Technol 2015;5:2587–91.
[8] Nuss KMR, von Rechenberg B. Biocompatibility issues with modern implants in bone - a review for clinical orthopedics. Open Orthop J 2008;2:66–78.
[9] Prasad K, Bazaka O, Chua M, Rochford M, Fedrick L, Spoor J, et al. Metallic biomaterials: current Challenges and Opportunities. Materials 2017;10:884.
[10] Wang W, Yeung KWK. Bone grafts and biomaterials substitutes for bone defect repair: a review. Bioact Mater 2017;2:224–47.
[11] Chen Y, Xu Z, Smith C, Sankar J. Recent advances on the development of magnesium alloys for biodegradable implants. Acta Biomater 2014;10:4561–73.
[12] Staiger MP, Pietak AM, Huadmai J, Dias G. Magnesium and its alloys as orthopedic biomaterials: a review. Biomaterials 2006;27:1728–34.
[13] Peuster M, Hesse C, Schloo T, Fink C, Beerbaum P, von Schnakenburg C. Long-term biocompatibility of a corrodible peripheral iron stent in the porcine descending aorta. Biomaterials 2006;27:4955–62.
[14] Li H, Zheng Y, Qin L. Progress of biodegradable metals. Prog Nat Sci: Mater Int 2014;24:414–22.
[15] Zartner P, Cesnjevar R, Singer H, Weyand M. First successful implantation of a biodegradable metal stent into the left pulmonary artery of a preterm baby Cathet Cardiovasc Interv 2005;66:590–4.
[16] Di Mario C, Griffiths H, Goktekin O, Peeters N, Verbist J, Bosiers M, et al. Drug-eluting bioabsorbable magnesium stent. J Intervent Cardiol 2004;17:391–5.
[17] Peeters P, Bosiers M, Verbist J, Deloose K, Heublein B. Preliminary results after application of absorbable metal stents in patients with critical limb ischemia. J Endovasc Ther 2005;12:1–5.
[18] Erbel R, Di Mario C, Bartunek J, Bonnier J, de Bruyne B, Eberli FR, et al. Temporary scaffolding of coronary arteries with bioabsorbable magnesium stents: a prospective, non-randomised multicentre trial. Lancet 2007;369:1869–75.
[19] Nielsen FH. Magnesium deficiency and increased inflammation: current perspectives. J Inflamm Res 2018;11:25–34.
[20] Abhinandan R, Adithya SP, Sidharthan DS, Balagangadharan K, Selvamurugan N. Synthesis and characterization of magnesium diboride nanosheets in alginate/polyvinyl alcohol scaffolds for bone tissue engineering. Colloids Surf B Biointerfaces 2021;203:111771.
[21] Batalu D, Stanciuc AM, Moldovan L, Aldica G, Badica P. Evaluation of pristine and Eu_2O_3-added MgB_2 ceramics for medical applications: hardness, corrosion resistance, cytotoxicity and antibacterial activity. Mater Sci Eng C 2014;42:350–61.
[22] Badica P, Batalu ND, Chifiriuc MC, Burdusel M, Grigoroscuta MA, Aldica G, et al. MgB_2 powders and bioevaluation of their interaction with planktonic microbes, biofilms, and tumor cells. J Mater Res Technol 2021;12:2168–84.
[23] Uluisik I, Karakaya HC, Koc A. The importance of boron in biological systems. J Trace Elem Med Biol 2018;45:156–62.
[24] Wolf FI, Cittadini A. Chemistry and biochemistry of magnesium. Mol Aspect Med 2003;24:3–9.
[25] Clarke WB, Webber CE, Koekebakker M, Barr RD. Lithium and boron in human blood. J Lab Clin Med 1987;109:155–8.
[26] Hunt CD. Regulation of enzymatic activity – one possible role of dietary boron in higher animals and humans. Biol Trace Elem Res 1998;66:205–25.
[27] Tanaka M, Fujiwara T. Physiological roles and transport mechanisms of boron: perspectives from plants. Pflugers Arch.-Eur. J. Physiol. 2008;456:671–7.
[28] Cui Y, Winton MI, Zhang ZF, Rainey C, Marshall J, De Kernion JB, et al. Dietary boron intake and prostate cancer risk. Oncol Rep 2004;11:887–92.
[29] Kot FS. Boron sources, speciation and its potential impact on health. Rev Environ Sci Biotechnol 2009;8:3–28.
[30] Nielsen FH. Boron in human and animal nutrition. Plant Soil 1997;193:199–208.
[31] Badica P, Batalu ND, Burdusel M, Grigoroscuta MA, Aldica G, Enculescu M, et al. Antibacterial composite coatings of MgB_2 powders embedded in PVP matrix. Sci Rep 2021;11:9591.
[32] Gheorghe I, Avram I, Corbu VM, Marutescu L, Popa M, Balotescu I, et al. In vitro evaluation of MgB_2 powders as novel tools to fight fungal biodeterioration of heritage buildings and objects. Frontiers in Materials 2021;7:601059.
[33] Erinc M, Sillekens WH, Mannens R, Werkhoven RJ. Applicability of existing magnesium alloys as biomedical implant materials. In: Nyberg EA, Agnew SR, Neelameggham NR, Pekguleryuz MQ, editors. Magnesium Technology. San Francisco; 2009. p. 209–14.
[34] Gao C, Li S, Liu L, Bin S, Yang Y, Peng S, et al. Dual alloying improves the corrosion resistance of biodegradable Mg alloys prepared by selective laser melting. J. Magnes. Alloy. 2021;9:305–16.
[35] Witte F, Hort N, Vogt C, Cohen S, Kainer KU, Willumeit R, et al. Degradable biomaterials based on magnesium corrosion. Curr Opin Solid State Mater Sci 2008;12:63–72.
[36] Batalu D, Bojin D, Ghiban B, Aldica G, Badica P. Corrosion behavior of pristine and added MgB_2 in phosphate buffered saline solution. IOP Conf Ser Mater Sci Eng 2012;40:012032.
[37] Cronin DS, Singh D, Gierczycka D, Barker J, Shen D. Modeling the neck for impact scenarios. In: Basic finite element method as applied to injury biomechanics. Academic Press; 2018. p. 503–38.
[38] Murakami A, Noudem J, Guesmi Z, Kudo T, Iwamoto A. Mechanical properties of MgB_2 bulk fabricated by spark plasma sintering. Phys Procedia 2015;65:77–80.
[39] Persaud-Sharma D, McGoron A. Biodegradable magnesium alloys: a review of material development and applications. J Biomim Biomater Tissue Eng 2012;12:25–39.
[40] Seal CK, Vince K, Hodgson MA. Biodegradable surgical implants based on magnesium alloys - a review of current research. IOP Conf Ser Mater Sci Eng 2009;4:012011.
[41] Salahshoor M, Guo Y. Biodegradable orthopedic magnesium-Calcium (MgCa) alloys, processing, and corrosion performance. Materials 2012;5:135–55.
[42] Badica P, Batalu D, Burdusel M, Grigoroscuta MA, Aldica GV, Enculescu M, et al. Compressive properties of pristine and SiC-Te-added MgB_2 powders, green compacts and spark-plasma-sintered bulks. Ceram Int 2018;44:10181–91.
[43] Shimada Y, Hata S, Ikeda K, Nakashima H, Matsumoto A, Togano K, et al. Infiltration behavior of molten Mg and its influence on microstructural evolution in SiC-doped MgB_2 wires prepared by internal Mg diffusion process. J Alloys Compd 2018;740:305–11.
[44] Giunchi G. High density MgB_2 obtained by reactive liquid Mg infiltration. Int J Mod Phys B 2003;17:453–60.
[45] Aldica G, Batalu D, Popa S, Ivan I, Nita P, Sakka Y, et al. Spark plasma sintering of MgB_2 in the two-temperature route. Phys C Supercond Appl 2012;477:43–50.
[46] Dai Z, Ronholm J, Tian Y, Sethi B, Cao X. Sterilization techniques for biodegradable scaffolds in tissue engineering applications. J Tissue Eng 2016;7:1–13.

[47] Frosch S, Nüsse V, Frosch KH, Lehmann W, Buchhorn G. Osseointegration of 3D porous and solid Ti–6Al–4V implants - narrow gap push-out testing and experimental setup considerations. J Mech Behav Biomed Mater 2021;115:104282.
[48] Seralp Uzun. Research on the development of medical-veterinary biotechnologies in bone healing using bioresorbable implants. USAMVB: Doctoral Thesis; 2019.
[49] Balint E. In: Ghid practic de hematologie și citologie veterinară (in Romanian); 2011. Curtea Veche, București, Romania.
[50] Piaton E, Fabre M, Goubin-Versini I, Bretz-Grenier M, Courtade-Saïdi M, Vincent S, et al. Recommandations techniques et règles de bonne pratique pour la coloration de May-Grünwald-Giemsa: revue de la littérature et apport de l'assurance qualité. Ann Pathol 2015;35(4):294–305.
[51] Sharkey L, Radin M, Seelig D. Veterinary cytology. 1st ed. Wiley-Blackwell; 2021. p. 12–4.
[52] Ordodi VL, Mic FA, Mic AA, Tanasie G, Ionac M, Sandesc D, et al. Bone marrow aspiration from rats: a minimally invasive procedure. Published online at, http://www.labanimal.com; 2006.
[53] Lindstrom NM, Moore DM, Zimmerman K, Smith SA. Hematologic assessment in pet rats, mice, hamsters, and gerbils: blood sample collection and blood cell identification. Vet Clin North Am Exot Anim Pract 2015 Jan;18(1):21–32.
[54] Bancroft JD, Gamble M. Theory and practice of histological techniques. 6th ed. Churchill Livingstone Elsevier Limited; 2008.
[55] Tiseanu I, Tsitrone E, Craciunescu T, Loarer T, Pegourie B, Dittmar T. X-ray micro-tomography studies on carbon based composite materials for porosity network characterization. Fusion Eng Des 2011;86:1646–51.
[56] Tiseanu I, Craciunescu T, Ruset C, Dobrea C, Sima A, Lungu M. Advanced X-ray imaging of metal coated/impregnated plasma-facing composite materials, 6th International Conference on Plasma Physics and Applications. Bucharest: Magurele; 2013. Romania.
[57] Witte F, Kaese V, Haferkamp H, Switzer E, Meyer-Lindenberg A, Wirth CJ, et al. Vivo corrosion of four magnesium alloys and the associated bone response. Biomaterials 2005;26:3557–63.
[58] Cifuentes SC, Amparo FB, Gallardo-Moreno M, Osswald TA, González-Carrasco JL, Benavente R, et al. Incorporation of Mg particles into PDLLA regulates mesenchymal stem cell and macrophage responses. J Biomed Mater Res A 2016;104:866–78.
[59] Zhang HY, Jiang HB, Kim J-E, Zhang S, Kim K-M, Kwon J-S. Bioresorbable magnesium-reinforced PLA membrane for guided bone/tissue regeneration. J Mech Behav Biomed Mater 2020;112:104061.
[60] Zimmermann T, Ferrandez-Montero A, Lieblich M, Ferrari B, González-Carrasco JL, Müller W-D, et al. In vitro degradation of a biodegradable polylactic acid/magnesium composite as potential bone augmentation material in the presence of titanium and PEEK dental implants. Dent Mater 2018;34:1492–500.
[61] Ferrández-Montero A, Lieblich M, González-Carrasco JL, Benavente R, Lorenzo V, Detsch R, et al. Development of biocompatible and fully biosabsorbable PLA/Mg films for tissue regeneration applications. Acta Biomater 2019;28:114–24.
[62] Fernández-Calderón MC, Romero-Guzmán D, Ferrández-Montero A, Pérez-Giraldo C, González-Carrasco JL, Lieblich M, et al. Impact of PLA/Mg films degradation on surface physical properties and biofilm survival. Colloids Surf, B 2020;185:110167.